Available online at website: https://journal.bcrec.id/index.php/jcerp

Journal of Chemical Engineering Research Progress, 3 (2) 2026, 289-299

Research Article

Study on the Model Prediction Control and MRAS in Electrodeposited Process Control System for Vehicle Painting

Jo Hyok*, Pak GumHyok, Ri CholMan, Han GuangJin, Kim Jong Chol, Ri Gi Song

Faculty of Control Science, University of Sciences, Unjong District, Pyongyang 999093, Democratic People's Republic of Korea.

Received: 11th May 2026; Revised: 10th June 2026; Accepted: 22th June 2026
Available online: 3rd July 2026; Published regularly: December 2026

Abstract

Electrodeposition is widely used in automotive painting due to its high adhesion and uniform coating. Temperature control is critical for coating quality, but stirred tanks exhibit nonlinear dynamics with large inertia and time-varying parameters. This study aims to develop an integrated control strategy combining model predictive control (MPC) with a model reference adaptive system (MRAS) to improve temperature control accuracy and robustness in a stirred electrodeposition tank. A robust MPC with N-step-free control action was designed based on an ARX-identified state-space model, and an MRAS estimator with PI adaptation was integrated to online-update the dominant time constant perturbed by stirring. Simulation and experimental results demonstrated that the proposed MPC-MRAS method achieved temperature control accuracy within ±0.2 °C, superior set-point tracking, and robust disturbance rejection compared to conventional MPC without parameter adaptation. The integrated strategy effectively compensates for model uncertainties caused by fluid agitation and operational variations, showing significant potential for industrial electrodeposition applications.

Keywords: Painting; Stirring; Temperature; Model predictive control; MRAS; Electrochemical reactor

How to Cite: Hyok, J., GumHyok, P., CholMan, R., GuangJin, H., Chol, K. J., Song, R. G. (2026). Study on the Model Prediction Control and MRAS in Electrodeposited Process Control System for Vehicle Painting. *Journal of Chemical Engineering Research Progress*, 3 (2), 289-299 (DOI: 10.9767/jcerp.20731)

Permalink/DOI: https://doi.org/10.9767/jcerp.20731

1. Introduction

Electrodeposition is a critical coating process widely employed in industrial manufacturing, particularly as a primer for automotive bodies, due to its ability to form uniform, pore-free, and highly adhesive films with minimal material loss [1,2]. The process involves the migration of charged paint particles in an aqueous solution towards a workpiece acting as an electrode under an applied electric field. The quality of the electrodeposited coating, including its thickness, uniformity, and corrosion resistance, is highly dependent on maintaining strict control over process parameters such as voltage, concentration, and temperature [3,4].

Among these parameters, bath temperature is paramount because it directly influences ion mobility, reaction kinetics, and the viscosity of the coating solution [5]. Precise temperature control is essential; low temperatures can increase viscosity and lead to incomplete coating formation, while excessively high temperatures may cause solvent loss, heterogeneous films, and pose safety risks. The industrial implementation of electrodeposition adds further complexity because continuous agitation is necessary to prevent solute sedimentation and temperature stratification, and the system is subject to significant disturbances, such as the loading and unloading of large chassis at ambient temperature. These factors transform

* Corresponding Author.
Email: jho9015@163.com (J. Hyok).

the electrodeposition tank into a complex thermal system with nonlinear dynamics, a large of inertial time constant, and significant parameter variations, making it a challenging control object [6].

Traditional control methods often struggle to provide satisfactory performance for such systems. Model Predictive Control (MPC) has emerged as a powerful advanced control strategy for processes with large time delays and inertia, as it uses an explicit model to predict future system behavior and computes optimal control actions by solving a finite-horizon optimization problem [7,8]. Since its industrial introduction in the late 1970s with algorithms such as IDCOM and DMC, MPC has evolved significantly, incorporating rigorous stability theory using Lyapunov functions and handling constraints explicitly through optimization [9]. Recent advances have extended MPC to electrochemical reactor systems, where machine learning techniques such as recurrent neural networks and physics-informed neural networks have been integrated to handle complex nonlinear dynamics and real-time optimization requirements [10,11].

However, the performance of MPC is inherently tied to the accuracy of its internal model. In a stirred electrodeposition tank, the effective thermal dynamics change significantly due to fluid mixing, leading to model uncertainties that can degrade the control performance of a standard MPC with a fixed model [12,13]. Recent research on electrochemical reactors has demonstrated that time-varying parameters and operational disturbances require adaptive mechanisms to maintain control performance. To address model-plant mismatch in coating processes, adaptive control strategies such as Model Reference Adaptive Systems (MRAS) have been successfully applied in thermal spray applications, where robust adaptation mechanisms compensate for process variations [14,15].

To address this challenge, this paper proposes a novel integrated control strategy that combines MPC with a Model Reference Adaptive System (MRAS). The core idea is to enhance the robustness of the MPC by incorporating an MRAS-based online parameter estimator, drawing from classical adaptive control theory [16,17]. The MRAS continuously identifies key system parameters, such as the dominant time constant, which are perturbed by the stirring action and operational changes. This estimated model is then fed into the MPC's predictor, effectively creating an adaptive predictive controller [18]. The proposed method ensures high temperature control accuracy and homogeneity despite model variations and external disturbances. By leveraging sparse identification techniques and machine learning-based state estimation [19], the control system can respond rapidly to fluctuations in process volume and maintain robustness against variations in coating fluid flow. Simulation and experimental results demonstrate that the combined MPC-MRAS approach significantly outperforms conventional MPC and decentralized control methods [20], offering superior set-point tracking and disturbance rejection, making it highly suitable for the temperature control of industrial electrodeposition systems.

2. Methods

2.1. Model Predictive Control (MPC)

Model Predictive Control (MPC) is an advanced control technique that utilizes an explicit dynamic model of the process to predict its future behavior over a finite horizon. The fundamental principle, illustrated in Figure 1, involves solving an online optimization problem at each sampling instant to determine a sequence of future control moves that minimize a predefined cost function, typically the error between the predicted output and a desired reference trajectory. Only the first control action in the optimized sequence is applied to the plant. At the next time step, the horizon is shifted, and the optimization is repeated with new measured data, in a so-called receding horizon strategy [7,8]. This feedback mechanism allows MPC to handle constraints on inputs and states explicitly and compensate for unmeasured disturbances. Fuzzy MPC algorithms have been proposed to handle the computational efficiency and prediction accuracy in chemical reactor applications [21].

The development of MPC can be traced through several key stages. The first industrial MPC algorithms, such as Identification and Command (IDCOM) and Dynamic Matrix Control (DMC), were developed in the late 1970s and early 1980s. They used finite impulse or step response

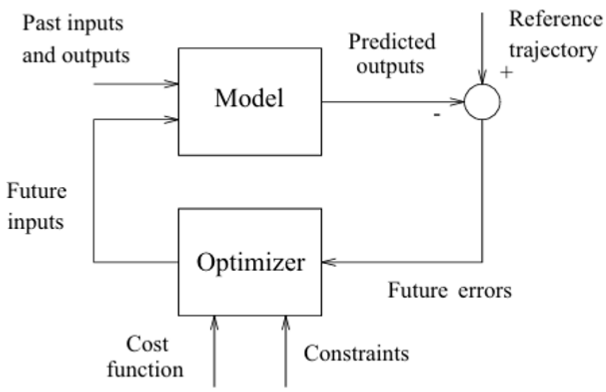

Figure 1. Basic structure of MPC.

models and employed quadratic programming to handle constraints. Generalized Predictive Control (GPC) emerged from the adaptive control community and used controlled auto-regressive integrated moving average (CARIMA) models, being particularly effective for systems without well-defined models. A significant theoretical advancement was the use of the value function from the finite-horizon optimal control problem as a Lyapunov function to guarantee closed-loop stability for constrained linear and nonlinear systems [8,9]. Recent developments have integrated machine learning techniques, including recurrent neural networks (RNN) and physics-informed neural networks (PINN), to enhance MPC performance in highly nonlinear electrochemical systems. These approaches enable real-time optimization and multivariable feedback control in complex electrochemical reactors [6,10].

For a discrete-time system model:

$$\begin{cases} x(k+1) = f(x(k), u(k)) \\ y(k) = h(x(k)) \end{cases} \tag{1}$$

subject to constraints $u(k) \in \mathrm{U}$ and $x(k) \in \mathbb{X}$, the MPC law is derived by solving the following problem at each time step k :

$$\min_{u} V(x,k,u) = \sum_{i=k}^{k+N-1} l(x(i),u(i)) + F(x(k+N)) \tag{2}$$

where $l(\cdot)$ is the stage cost, $F(\cdot)$ is the terminal cost, and N is the prediction horizon.

2.2. Robust MPC (RMPC) and Problem Formulation

For systems with significant model uncertainties, such as the electrodeposition tank, a Robust MPC (RMPC) approach is necessary. Recent research has demonstrated the effectiveness of RMPC in electrochemical systems where model uncertainties and disturbances are prevalent [19]. Specifically, MPC strategies have been successfully applied to electrically-heated steam methane reformers [22], demonstrating robust performance in high-temperature electrochemical environments. Consider a linear system with polytopic or structured uncertainty:

$$x(k+1) = A(k)x(k) + B(k)u(k) \tag{3}$$

where $[A(k), B(k)]$ belong to a known uncertainty set. The objective of RMPC is to design a controller that minimizes the worst-case performance cost while satisfying all constraints for all possible model realizations [23].

A common RMPC formulation involves a min-max optimization problem:

$$\min_{U(k)} \max_{[A(k),B(k)]} J(k) = \sum_{i=0}^{\infty} [x(k+i \mid k)^T Q x(k+i \mid k) + u(k+i \mid k)^T R u(k+i \mid k)] \tag{4}$$

where $Q > 0$ and $R > 0$. To make this problem tractable, a typical strategy is to use a free control sequence over an initial horizon followed by a fixed state feedback law. Using Lyapunov stability theory and the S-procedure, the constraints and stability conditions can be transformed into a set of Linear Matrix Inequalities (LMIs) that can be solved efficiently [23,24]. This LMI-based approach ensures robust stability and constraint satisfaction for the electrodeposition tank control system.

2.3. Model Reference Adaptive System (MRAS)

The Model Reference Adaptive System (MRAS) is a framework for online parameter estimation in adaptive control [16,17]. The core idea is to adjust the parameters of an adjustable model so that its output converges to the output of a reference model (or the actual plant). The parameter adjustment mechanism is driven by the error between the two outputs. In industrial coating applications, MRAS has been successfully employed to control atmospheric plasma spray processes, where robust model reference adaptive controllers maintain consistent mean particle states despite process uncertainties [14,15]. Furthermore, feedback control designs for such coating processes must account for distributed parameters like powder size to achieve consistent deposition quality [24]. These applications demonstrate that MRAS can effectively handle the model variations inherent in thermal and coating processes.

In this work, MRAS is employed to estimate the dominant time constant of the electrodeposition tank, which varies due to stirring and fluid mixing. The plant is approximated by a first-order plus time delay model:

$$G_p(s) = \frac{K}{Ts+1} e^{-\tau s} \tag{5}$$

The MRAS structure uses the actual plant as the reference model and an adjustable first-order model. The error $e = y - \hat{y}$ between the actual tank temperature y and the estimated temperature $\hat{y}$ is fed to a Pl adaptation mechanism to update the estimated time constant $\hat{T}$. This onlineestimated parameter is used to adapt the prediction model in the MPC algorithm, similar to adaptive mechanisms used in thermal barrier coating processes [14].

2.4. Problem Formulation for the Electrodeposition Tank

The specific control problem addressed is to maintain the temperature of a stirred electrodeposition tank at a precise set-point despite significant model uncertainties arising from complex, agitation-dependent heat exchange dynamics [2,3], time-varying parameters (e.g., the system's time constant) due to operational changes like fluid circulation and chassis loading [6], and input constraints on the heater voltage. These modeling challenges are analogous to those encountered in other industrial coating systems, where multi-scale modeling approaches have proven essential for capturing both macroscopic and microscopic process dynamics [25]. The proposed solution is an integrated RMPC strategy where the MRAS algorithm provides real-time estimates of the critical plant parameter (time constant). This estimated parameter is used to adapt the prediction model within the RMPC framework, which is formulated as an LMI optimization problem to ensure robust constraint satisfaction and stability [22,23]. This approach combines the predictive capabilities of MPC with the adaptive robustness of MRAS, addressing the challenges identified in recent studies on electrochemical reactor control.

3. Results and Discussion

3.1. Model Predictive Control System Design with MRAS Modeling

The schematic of the electrodeposition process with modeling stirrer is shown in Figure 2. The operating volume of the predictive controller used for the temperature control of the electrodeposition tank is the voltage of the electric heater, in addition to the system that combines the motor control for the agitation of the solution and the valve control for the concentration and level of the electrodeposition solution. This paper deals with the temperature control process.

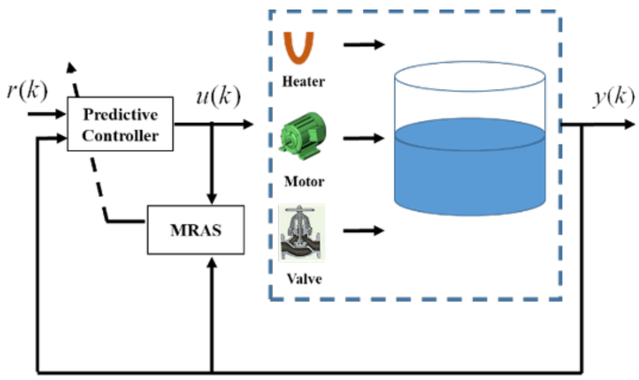

Figure 2. Schematic diagram of electrodeposition tank temperature control system with stirrer.

The configuration of the electrodeposition tank temperature control system with a stirrer can generally be represented by the ARX model as follows:

$$y(t) + a_1 y(t-1) + \cdots + a_{ny} y(t-ny) = b_1 u(t-nk) + \cdots + b_{nb} u(t-nu-nk+1) + e(t) \quad (6)$$

where nk is the delay of the object and is the white noise applied to the object.

The heat exchange process in the electrodeposition tank is a complex nonlinear and uncertain process due to the action of the stirrer and the motor valve. Due to the difficulty of analytical modeling, we used MATLAB to obtain the mathematical model of the plant with the ARX model from the measured data of the actual process. In order for the system to be identifiable, the input signal must excite all the natural modes of the identified object sufficiently, and the input signal is applied to the object to meet the continuous excitation condition. From the sampling theorem, the sampling interval was set to 5 s less than half of the effective maximum high-frequency component period. The temperatures measured in real time by the Pt100 sensor and the heater terminal voltage measured in real time are stored in real time in the PLC data register. The number of data used for identification in each interval is 300, and the total number of data used for identification is 3000.

The identification model obtained is as follows:

$$A_1(q) = 1 - 0.6986q^{-1} - 0.2751q^{-2} - 0.07925q^{-3} + 0.03425q^{-4}$$
$$B_1(q) = 0.0001551q^{-1} \quad (7)$$

$$A_2(q) = 1 - 0.6963q^{-1} - 0.2852q^{-2} - 0.08332q^{-3} + 0.03616q^{-4}$$
$$B_2(q) = 0.0001475q^{-1} \quad (8)$$

$$A_3(q) = 1 - 0.7659q^{-1} - 0.2602q^{-2} - 0.08165q^{-3} + 0.03256q^{-4}$$
$$B_3(q) = 0.0001528q^{-1} \quad (9)$$

$$A_4(q) = 1 - 0.7145q^{-1} - 0.2675q^{-2} - 0.08256q^{-3} + 0.03276q^{-4}$$
$$B_4(q) = 0.0001412q^{-1} \quad (10)$$

$$A_5(q) = 1 - 0.7546q^{-1} - 0.2888q^{-2} - 0.07644q^{-3} + 0.03451q^{-4}$$
$$B_5(q) = 0.0001519q^{-1} \quad (11)$$

To make a given ARX model a state-space model, we set the state to:

$$x(t) = [y(t), y(t-1), y(t-2), y(t-3)]^T \quad (12)$$

Then, the state-space model is:

$$x(t+1) = \begin{bmatrix} -a_1 & -a_2 & -a_3 & -a_4 \\ 1 & 0 & 0 & 0 \\ 0 & 1 & 0 & 0 \\ 0 & 0 & 1 & 0 \end{bmatrix} x(t) + \begin{bmatrix} b_1 \\ 0 \\ 0 \\ 0 \end{bmatrix} u(t) \tag{13}$$

$$y(t) = [1 \quad 0 \quad 0 \quad 0]x(t) \tag{14}$$

From this, the state-space model of an object is obtained as:

$$A_1 = \begin{bmatrix} 0.6986 & 0.2751 & 0.07925 & -0.03425 \\ 1 & 0 & 0 & 0 \\ 0 & 1 & 0 & 0 \\ 0 & 0 & 1 & 0 \end{bmatrix} \tag{15}$$

$$B_1 = [0.0001551 \quad 0 \quad 0 \quad 0]^T \tag{16}$$

$$A_2 = \begin{bmatrix} 0.6963 & 0.2852 & 0.08332 & -0.03616 \\ 1 & 0 & 0 & 0 \\ 0 & 1 & 0 & 0 \\ 0 & 0 & 1 & 0 \end{bmatrix} \tag{17}$$

$$B_2 = [0.0001475 \quad 0 \quad 0 \quad 0]^T \tag{18}$$

$$A_3 = \begin{bmatrix} 0.7659 & 0.2602 & 0.08165 & -0.03256 \\ 1 & 0 & 0 & 0 \\ 0 & 1 & 0 & 0 \\ 0 & 0 & 1 & 0 \end{bmatrix} \tag{19}$$

$$B_3 = [0.0001528 \quad 0 \quad 0 \quad 0]^T \tag{20}$$

$$A_4 = \begin{bmatrix} 0.7145 & 0.2675 & 0.08256 & -0.03276 \\ 1 & 0 & 0 & 0 \\ 0 & 1 & 0 & 0 \\ 0 & 0 & 1 & 0 \end{bmatrix} \tag{21}$$

$$B_4 = [0.0001412 \quad 0 \quad 0 \quad 0] \tag{22}$$

$$A_5 = \begin{bmatrix} 0.7546 & 0.2888 & 0.07644 & -0.03451 \\ 1 & 0 & 0 & 0 \\ 0 & 1 & 0 & 0 \\ 0 & 0 & 1 & 0 \end{bmatrix} \tag{23}$$

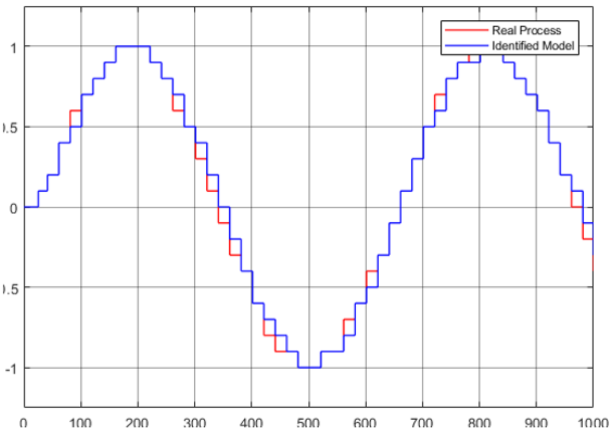

Figure 3. Model verification.

The comparison curve between the identified model and the normalized temperature measurement is shown in Figure 3. As shown in the figure, it can be seen that the output of the model obtained by identification is in close agreement with the actual measurements of the plant. It can be seen that the obtained model accurately reflects the dynamic characteristics of the plant.

3.2. Design of Control System

In this section, we first derive a RMPC algorithm with N-step-free control action as an online RMPC based on the structured model uncertainty representation. The online RMPC designed in this paper has high optimality so that the temperature deviations caused by the loading of the chassis or the electrodeposition injection can be restored to the set point in time. Then, based on the structured model uncertainty representation, an offline RMPC algorithm is derived. In general, the RMPC design has to solve the following optimization problem at each sampling time k:

$$\min_{U(k)} \max_{[A(k),B(k)]} J(k) \tag{24}$$

Here,

$$J(k) = \sum_{i=0}^{\infty}[x(k+i|k)^T Q_1 x(k+i|k) + u(k+i|k)^T R u(k+i|k)] \tag{25}$$
$$Q_1 > 0,\ R > 0$$

Before computing the state feedback matrix, the N-step-free control action is determined first and then finding the state feedback matrix to improve the optimality of the controller is a fundamental feature of this controller. By N-step-free control action and state feedback matrix at each sampling time, the control input is given by:

$$U(k) = \begin{cases} u(k+i|k), & 0 \le i \le N \\ F(k)x(x+i|k), & i \ge N \end{cases} \tag{26}$$

Then the optimization problem is divided into two parts as follows:

$$\min_{u(k+i|k)} \max_{[A(k),B(k)]} J_0(k)$$
$$J_0 = \sum_{i=0}^{N-1} x(k+i|k)^T Q_1 x(k+i|k) + u(k+i|k)^T R u(k+i|k) \tag{27}$$

$$\min_{F(k)x(k+i|k)} \max_{[A(k),B(k)]} J_1(k)$$
$$J_1 = \sum_{i=N}^{\infty} x(k+i|k)^T Q_1 x(k+i|k) + u(k+i|k)^T R u(k+i|k) \tag{28}$$

Assume the quadratic function with respect to the state x(k) of the system for $\forall k, \forall i \geq N, P(k) \geq 0$:

$$V(x(k+i|k)) = x(k+i|k)^T P(k) x(k+i|k) \tag{29}$$

$V(x)$ satisfies the following condition:

$$V(x(k+i+1|k)) - V(x(k+i|k)) \leq -[x(k+i|k)^T Q_1 x(k+i|k) + u(k+i|k)^T R x(k+i|k)] \tag{30}$$

Summing the inequality (30) from i = N to i = ∞, we obtain:

$$J_1(k) \leq V(x(k+N)) = x(k+N|k)^T P(k) x(k+N|k) \tag{31}$$

Then it is easy to see that the following inequality holds:

$$\bar{J}(k) = \sum_{i=0}^{N-1}[x(k+i|k)^T Q_1 x(k+i|k) + u(k+i|k)^T R u(k+i|k)] + V(x(k+N|k)) \geq J(k) \tag{32}$$

The prediction of the state is given by:

$$\begin{bmatrix} x(k+1|k) \\ \vdots \\ x(k+N|k) \end{bmatrix} = \begin{bmatrix} A(k) \\ \vdots \\ A(k+N-1)\cdots A(k+1)A(k) \end{bmatrix} x(k)$$
$$+$$
$$+$$
$$\begin{bmatrix} B(k) & 0 & \cdots & 0 \\ \vdots & \ddots & & \\ \vdots & & \ddots & \\ A(k+N-1)\cdots A(k+1)B(k) & \cdots & \cdots & B(k+N-1) \end{bmatrix} \begin{bmatrix} u(k|k) \\ \vdots \\ \vdots \\ u(k+N-1|k) \end{bmatrix} \tag{33}$$

The expression (33) can be simply written as:

$$\begin{bmatrix} \tilde{x}(k) \\ x(k+N|k) \end{bmatrix} = \begin{bmatrix} \tilde{A}(k) \\ \tilde{A}_N(k) \end{bmatrix} x(k) + \begin{bmatrix} \tilde{B}(k) \\ \tilde{B}_N(k) \end{bmatrix} \tilde{u}(k) \tag{34}$$

Here,

$$\tilde{A}(k) = \begin{bmatrix} A(k) \\ \vdots \\ A^{N-1}(k) \end{bmatrix} \tag{35}$$

$$\tilde{B}(k) = \begin{bmatrix} B(k) & 0 & \cdots & 0 \\ \vdots & & & \\ \vdots & & & \\ A^{N-2}(k)B(k) & \cdots & \cdots & 0 \end{bmatrix} \tag{36}$$

$$\tilde{A}_N(k) = A^N(k) \tag{37}$$
$$\tilde{B}_N(k) = [A^{N-1}(k)B(k) \quad \cdots \quad B(k)] \tag{38}$$

$$\tilde{x}(k) = \begin{bmatrix} x(k+1|k) \\ x(k+2|k) \\ \vdots \\ x(k+N-1|k) \end{bmatrix}, \ \tilde{u} = \begin{bmatrix} u(k|k) \\ \vdots \\ u(k+N-1|k) \end{bmatrix} \tag{39}$$

We assume that the system matrices A and B are constant matrices at each sampling time k. Then Eq. (32) can be rewritten as:

$$\bar{J}(k) = \|x(k)\|_{Q_1}^2 + \left\|\tilde{A}x(k) + \tilde{B}\tilde{u}\right\|_{\tilde{Q}}^2 + \|\tilde{u}\|_{\tilde{R}}^2 + \|x(k+N|k)\|_{P(k)}^2 \tag{40}$$

where $\tilde{Q}$ and $\tilde{R}$ are block diagonal matrices such that the *(i, i)* th block is Q_1, R. $\tilde{Q}$ consists of N-1 blocks and $\tilde{R}$ has N blocks. Now let η_1, η_2 be such that the following inequality holds. Then, the optimization problem of RMPC with N-step-free control action can be rewritten as (41):

$$\eta_1 \geq \left\|\tilde{A}x(k) + \tilde{B}\tilde{u}\right\|_{\tilde{Q}}^2 + \|\tilde{u}\|_{\tilde{R}}^2 \tag{41}$$
$$\eta_2 \geq \|x(k+N|k)\|_P^2 \tag{42}$$

where $\|x(k)\|_{Q_1}^2$ is given as a constant at sampling time k, and can therefore be omitted from the upper bound of the RMPC objective function.
Applying Schur's lemma, convert (31), (41), (42) to LMI.

[Lemma] Given matrices A, D, E, F with appropriate dimensions, let the matrix F satisfy $\|F\| \leq 1$
Then the following inequality holds for any symmetric matrix $P = P^T$ and $\varepsilon > 0$ such that $P - \varepsilon DD^T > 0$.

$$(A + DFE)^T P^{-1} (A + DFE) < A^T (P - \varepsilon DD^T)^{-1} A + 1/\varepsilon E^T E \tag{43}$$

Substituting Eqs. (13) and (15) into Eq. (31), we obtain:

$$\Delta V(x(k+i|k)) = x(k+i|k)^T\{-P + [A + BF + HF_1(k)(E_1 + E_2F)]^T * P[A + BF + HF_1(k)(E_1 + E_2F)]\}x(k+i|k) \tag{44}$$

From the above expression, (31) can be rewritten as:

$$x(k+i|k)^T M x(k+i|k) \leq 0 \tag{45}$$

Where, $M = -P + Q_1 + F^T R F + [A + BF + HF_1(k)(E_1 + E_2F)]^T P [A + BF + HF_1(k)(E_1 + E_2F)]$

From the lemma, we can see that the following inequality holds when (46) holds:

$$P^{-1} - \varepsilon HH^T > 0 \tag{46}$$

$$M \le -P + Q_1 + F^T RF + (A+BF)^T (P^{-1} - \varepsilon HH^T)^{-1}(A+BF) + 2\varepsilon^{-1}(E_1 + E_2F)^T(E_1+E_2F) \tag{47}$$

From (47) it can be seen that the inequality (31) holds if the following inequality holds:

$$-P + Q_1 + F^T RF + (A+BF)^T (P^{-1} - \varepsilon HH^T)^{-1}(A+BF) + 2\varepsilon^{-1}(E_1 + E_2F)^T(E_1+E_2F) \le 0 \tag{48}$$

Converting (49) to the LMI form, we have the following inequality $Q = \eta_2 P^{-1} > 0$, $F(k) = YQ^{-1}$, $\eta_2 \varepsilon = \lambda$:

$$\begin{bmatrix} Q & * & * & * & * \\ Q_1^{1/2}Q & \eta_2 & * & * & * \\ R^{1/2}Y & 0 & \eta_2 & * & * \\ E_1Q + E_2Y & \vdots & 0 & \lambda & * \\ AQ + BY & 0 & 0 & 0 & Q - \lambda HH^T \end{bmatrix} \ge 0 \tag{49}$$

Converting Eq. (35) to the LMI form, we obtain the following inequality:

$$\begin{bmatrix} \eta_1 & * & * \\ \tilde{u} & \tilde{R}^{-1} & * \\ \tilde{A}x(k) + \tilde{B}\tilde{u} & 0 & \tilde{Q}^{-1} \end{bmatrix} \ge 0 \tag{50}$$

As can be seen from (50), (35) and (36), we can find $\tilde{A}$, $\tilde{B}$, by $A(k)$, $B(k)$.

From the above considerations, the N-step-free control action RMPC controller design problem can be formulated as follows:
If there exist variables $\eta_1 > 0$, $\eta_2 > 0$, $\lambda > 0$, N-step-free control actions $u(k|k), \cdots, u(k+N-1|k)$ and symmetric matrices $Q > 0$and matrix Y that satisfy the following optimization problem, then there exist N-step-free control actions $u(k|k), \cdots, u(k+N-1|k)$ that minimize the upper bound of the RMPC objective function $F(k) = YQ^{-1}$:

$$\min_{\eta_1, \eta_2, u(k|k), \ldots, u(k+N-1|k), Y, Q, \lambda} \eta_1 + \eta_2 \tag{51}$$

$$0 \le u(k) \le 100 k = 0,1, \cdots, N-1$$

$$\begin{bmatrix} 10^4 & Y \\ Y^T & Q \end{bmatrix} \ge 0 \tag{52}$$

$$\begin{bmatrix} Q & * & * & * & * \\ Q_1^{1/2}Q & \eta_2 & * & * & * \\ R^{1/2}Y & 0 & \eta_2 & * & * \\ E_1Q + E_2Y & \vdots & 0 & \lambda & * \\ AQ + BY & 0 & 0 & 0 & Q - \lambda HH^T \end{bmatrix} \ge 0$$

$$\begin{bmatrix} \eta_1 & * & * \\ \tilde{u} & \tilde{R}^{-1} & * \\ \tilde{A}_S x(k) + \tilde{B}_S\tilde{u} & 0 & \tilde{Q}^{-1} \end{bmatrix} \ge 0$$

$$\begin{bmatrix} \eta_1 & * & * \\ \tilde{u} & \tilde{R}^{-1} & * \\ \tilde{A}_{tm} x(k) + \tilde{B}_{tm}\tilde{u} & 0 & \tilde{Q}^{-1} \end{bmatrix} \ge 0$$

$$\begin{bmatrix} 1 & * \\ \tilde{A}_{N,S} x(k) + \tilde{B}_{N,S}\tilde{u}(k) & Q \end{bmatrix} \ge 0$$

$$\begin{bmatrix} 1 & * \\ \tilde{A}_{N,tm} x(k) + \tilde{B}_{N,tm}(k)\tilde{u}(k) & Q \end{bmatrix} \ge 0$$

$$\begin{bmatrix} Q & * \\ H^T & \lambda^{-1} \end{bmatrix} > 0$$

3.2.1. Robust Stability

From Equation (51), the RMPC algorithm obtained from the optimization problem ensures the stability of the exponential closed-loop system of the stabilizable plant once the solution of the optimization problem exists. Assume that there exists a valid solution $\{\tilde{u}^*(k), F^*(k), P^*(k)\}$ at sampling time k!
Then, at time t, the following solution is valid:

$$u(k+i+1|k+1) = u^*(k+i+1|k),\ i = 0, \cdots, N-2 \tag{53}$$

$$u(k+i+N|k+1) = F^*(k)x^*(k+i+N|k) \tag{54}$$

Substituting Eq. (53) and (54) into (32), we obtain:

$$\bar{J}(k+1) = \sum_{i=0}^{N-1}[\|x(k+i+1|k)\|_{Q_1}^2 + \|u(k+i+1|k+1)\|_R^2] + \|x(k+N+1|k+1)\|_{P(k+1)}^2 == \sum_{i=1}^{N-1}[\|x^*(k+i|k)\|_{Q_1}^R + \|u^*(k+i|k)\|_R^2] + \|x^*(k+N|k)\|_{Q_1}^2 + \|u^*(k+N|k)\|_R^2 + \|x^*(k+N+1|k)\|_{P^*(k)}^2 \tag{55}$$

where

$$u^*(k+N|k) = F^*(k)x(k+N|k)$$

Considering Eq. (34) and (35), we have:

$$\|x^*(k+N+1|k)\|_{P^*(k)}^2 \le \|x^*(k+N|k)\|_{P^*(k)}^2 - \|x^*(k+N|k)\|_{Q_1}^2 - \|u^*(k+N|k)\|_R^2 \tag{56}$$

Substituting Eq. (56) into Eq. (55), we obtain:

$$\bar{J}(k+1) \le \sum_{i=1}^{N-1}[\|x^*(k+i|k)\|_{Q_1}^2 + \|u^*(k+i|k)\|_R^2] + \|x^*(k+N|k)\|_{P^*(k)}^2 \le \bar{J}^*(k) \tag{57}$$

Solving the optimization problem at time k+1 leads to $\bar{J}^*(k+1) \le \bar{J}(k+1)$.
Therefore, $\bar{J}^*(k)$ is a Lyapunov function and robust stability is guaranteed.

3.2.2. MRAS algorithm

In model predictive control, the accurate identification of the plant model is an important factor to ensure the quality of control. Of course, RMPC guarantees good robustness, but if the nominal model and the actual plant are severely different, the control error cannot be avoided. In this paper, the MRAS algorithm is used to estimate the inertial time constant of the control plant in the electrodeposition tank temperature control system. In general, the temperature control system is characterized by a large time constant, whereas in the electrodeposition tank control system, the inertia time constant is severely fluctuating due to external effects such as mixing of the stirrer and mixing of the solution in the replenishment tank (tank 2). The variation of the inertia time constant affects the coefficients, which are the largest contributing factors in Eq. (6). We have constructed the following MRAS identifier for identification of the inertial time constant. The block diagram of MRAS observer is shown in Figure 4.

In this paper, instead of the reference model, a real object (electrodeposition tank) is used, and an adaptive model is used, which is represented by a first-order inertial form with the following delay:

$$G_p(s) = \frac{k}{Ts+1} e^{-\tau s} \tag{58}$$

where T is the time constant of the electrodeposition tank, k is the gain, and is the delay time constant. By inputting the manipulated variable (voltage) applied to the electrodeposition tank into the adaptive model, the estimated value of the control variable ($\hat{y}$) is obtained and the error with the actual value (y) is used to estimate the time constant in the adaptive mechanism. The estimation of the time constant was performed using the PI algorithm.

$$\hat{T} = k_p e + \frac{k_i}{s} e$$

where e is the estimation error denoted by $e = y - \hat{y}$and k_p, k_i is the integral and derivative coefficients. The details are shown in the simulation results:

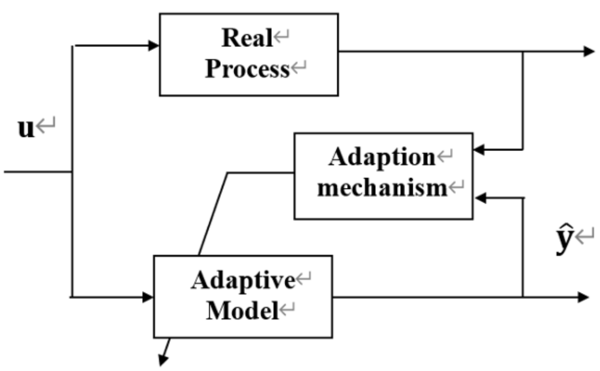

Figure 4. Block diagram of MRAS.

RMPC algorithm of the electrodeposition tank temperature control system

Offline part

Given the initial allowable state x_1, a sequence of minima γ_i, L_i, Y_i $(i = 1, \cdots, M)$ is generated as follows:

Step 1: Set the value of $i = 1, x_i = 1, N$.

Step 2: Solve the LMI optimization problem with additional constraints $L_{i-1} > L_i$ (only for $i \geq 2$) to compute the minimization γ_i, L_i, Y_i and store L_i^{-1}, $F_i(= Y_i L_i^{-1})$ in the lookup table.

Step 3: Choose a state x_{i+1} satisfying $\|x_{i+1}\|^2_{L_i^{-1}} < 1$

We go to step 2.

Online part

(1) $x(k)$ satisfies $\|x(k)\|^2_{L_i^{-1}} \leq 1$, computes the maximum index i such that $\|x(k)\|^2_{L_i^{-1}} \leq 1$

And we enforce the control law:

$u(k) = F_i(k)x(k)$

If $x(k)$ is not satisfied $\|x(k)\|^2_{L_i^{-1}} \leq 1$, we perform the RMPC algorithm with N-step-free control action.

(2) Measure $x(k+1)$ and go to (1).

3.3. Simulation and Experimental Results

The parameters of the electrodeposition process are shown in Table 1. The weight matrices of RMPC with N-step-free control action are defined appropriately. We compute the off-line part by using the mincx command in MATLAB with N = 5. Parameters of the electrodeposition process is shown in Table 1.

The weight matrices N and N of RMPC with N-step-free control action are defined as follows:

$$Q_1 = \begin{bmatrix} 50 & 0 & 0 & 0 \\ 0 & 50 & 0 & 0 \\ 0 & 0 & 50 & 0 \\ 0 & 0 & 0 & 50 \end{bmatrix}, \qquad R = 0.1, N = 5$$

We compute the off-line part by using the *mincx* command in MATLAB with N=5, $x_1 = [0.5 \quad 0.5 \quad 0.5 \quad 0.5]$.

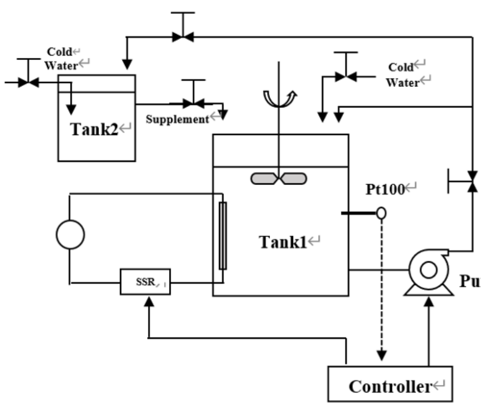

Figure 5. Schematic diagram of the electrodeposition tank control system.

$$L_1^{-1} = \begin{bmatrix} 1.6653 & 0.2546 & 0.0996 & -0.0326 \\ 0.2546 & 0.8349 & 0.0379 & -0.0114 \\ 0.0996 & 0.0379 & 0.5103 & -0.0046 \\ -0.0326 & -0.0114 & -0.0046 & 0.2473 \end{bmatrix},$$

$$\lambda(L_1^{-1}) = \begin{bmatrix} 0.2465 \\ 0.5009 \\ 0.7634 \\ 1.747 \end{bmatrix}$$

$$F_2 = [19.0345 \quad 28.791 \quad 39.8714 \quad 31.2746]$$

$$L_2^{-1} = \begin{bmatrix} 1.9986 & 0.3051 & 0.1194 & -0.0392 \\ 0.3051 & 1.0014 & 0.045 & -0.0139 \\ 0.1194 & 0.045 & 0.612 & -0.0058 \\ -0.0392 & -0.0139 & -0.0058 & 0.2966 \end{bmatrix},$$

$$\lambda(L_2^{-1}) = \begin{bmatrix} 0.2956 \\ 0.6007 \\ 0.9158 \\ 2.0964 \end{bmatrix}$$

$$F_2 = [22.0262 \quad 32.5693 \quad 45.1358 \quad 35.1195]$$

$$L_3^{-1} = \begin{bmatrix} 2.2207 & 0.3393 & 0.133 & -0.0436 \\ 0.3393 & 1.1125 & 0.0502 & -0.0153 \\ 0.133 & 0.0502 & 0.6799 & -0.0064 \\ -0.0436 & -0.0153 & -0.0064 & 0.3295 \end{bmatrix},$$

$$\lambda(L_3^{-1}) = \begin{bmatrix} 0.3284 \\ 0.6674 \\ 1.0173 \\ 2.3296 \end{bmatrix}$$

$$F_3 = [26.5143 \quad 38.8678 \quad 51.8696 \quad 40.2327]$$

$$L_4^{-1} = \begin{bmatrix} 2.4985 & 0.3813 & 0.1494 & -0.0491 \\ 0.3813 & 1.2509 & 0.056 & -0.0174 \\ 0.1494 & 0.056 & 0.7645 & -0.0074 \\ -0.0491 & -0.0174 & -0.0074 & 0.3706 \end{bmatrix},$$

$$\lambda(L_4^{-1}) = \begin{bmatrix} 0.3693 \\ 0.7504 \\ 1.1441 \\ 2.6206 \end{bmatrix}$$

$$F_4 = [28.7224 \quad 40.8244 \quad 55.0428 \quad 42.5888]$$

Table 1. Parameters of electrodeposition

No	Parameter	Value
1	Volume of tank 1	13 m^3
2	Volume of tank 2	1 m^3
3	Cold water temperature	20 ℃
4	Set point of temperature	45 ℃
5	Power voltage	AC 380V
6	Level	2 m
7	Heater capacity	40 kw

$$L_5^{-1} = \begin{bmatrix} 2.8544 & 0.437 & 0.1708 & -0.0558 \\ 0.437 & 1.4321 & 0.0656 & -0.0194 \\ 0.1708 & 0.0656 & 0.8754 & -0.0076 \\ -0.0558 & -0.0194 & -0.0076 & 0.4241 \end{bmatrix},$$

$$\lambda(L_5^{-1}) = \begin{bmatrix} 0.4227 \\ 0.8591 \\ 1.3092 \\ 2.995 \end{bmatrix}$$

$$F_5 = [33.2215 \quad 52.6422 \quad 73.0516 \quad 57.4571]$$

The simulation results of temperature control of the electrodeposition tank using conventional model predictive control (without MRAS) are shown in Figure 6. The simulation results of temperature control of electrodeposition tank using model predictive control with MRAS are shown in Figure 7. In a temperature control system with a relatively large time constant, the model predictive control shows a relatively good performance, but in a process with simultaneous stirring, such as an electrodeposition tank, there is a degradation due to model fluctuations. Figure 6 shows that the real-time model identification using the MRAS proposed in this paper significantly improves the temperature control accuracy. The results relate directly to the original objectives outlined in the Introduction section. The objective was to develop an integrated MPC-MRAS strategy to improve temperature control accuracy and robustness in a stirred electrodeposition tank. The findings demonstrate that the proposed method achieves this objective by maintaining temperature control accuracy within ±0.2 °C despite disturbances such as cold-water injection and heat dissipation to the outside. The scientific interpretation of these results is supported by the ARX model identification and the LMI-based RMPC formulation, which ensures robust stability and constraint satisfaction. The MRAS estimator with

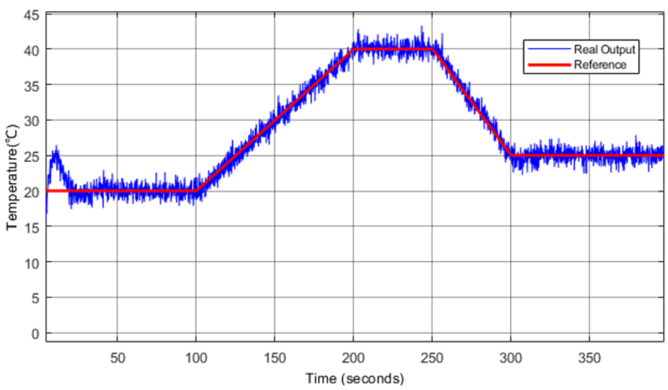

Figure 6. Simulation results of temperature control of electrodeposition tank using conventional model predictive control (without MRAS).

PI adaptation effectively compensates for the time-varying dominant time constant caused by fluid agitation, which is the primary source of model uncertainty in this system.

Compared with conventional MPC methods without parameter adaptation [16,17], the proposed MPC-MRAS method demonstrates superior performance in terms of high accuracy and robustness. The results are consistent with findings from other investigators who have applied adaptive control strategies to coating processes. For example, Guduri and Batra [2, 3] demonstrated that MRAS-based controllers can maintain consistent mean particle states in atmospheric plasma spray processes despite disturbances. Similarly, Luo et al. [1] showed that machine learning-based predictive control with online model linearization can effectively handle process variability in electrochemical reactors. The key difference in this work is the specific integration of MRAS with RMPC for temperature control in a stirred electrodeposition tank, where the time constant variation due to agitation is the critical challenge. While previous studies focused on concentration or particle state control [1, 7, 9], this work addresses the unique thermal dynamics of stirred tanks with large inertia and time-varying parameters.

4. Conclusions

This paper proposed an integrated MPC-MRAS strategy for precise temperature control of a stirred electrodeposition tank. The MRAS-based online parameter estimator effectively compensated for model uncertainties caused by fluid agitation, enhancing the adaptability of the predictive controller. Simulation results demonstrated that the proposed method outperformed conventional MPC by achieving superior set-point tracking (±0.2 °C accuracy) and robust disturbance rejection against operational variations such as chassis loading. The method shows significant potential for improving coating quality in industrial electrodeposition processes. Future work will focus on extending the proposed approach to multivariable control of voltage, concentration, and temperature simultaneously, and on implementing the algorithm in real-time industrial PLC systems.

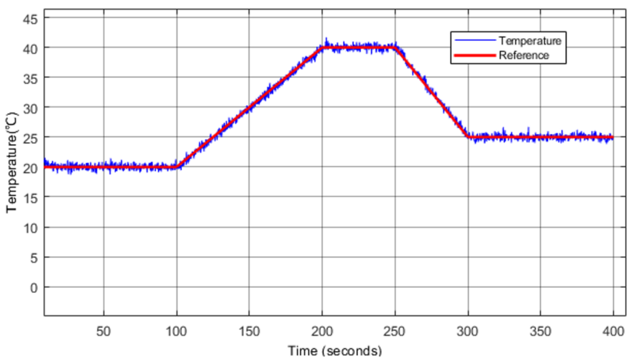

Figure 7. Simulation results of temperature control of electrodeposition tank using model predictive control with MRAS.

CRedit Authors Statement

Author Contributions: Jo Hyok: Conceptualization, Methodology, Software, Investigation, Writing - Original Draft, Writing - Review & Editing, Supervision; Pak GumHyok: Methodology, Software, Validation, Investigation, Data Curation, Writing - Original Draft; Ri CholMan: Investigation, Resources, Data Curation, Visualization; Han GuangJin: Investigation, Resources, Visualization; Kim JongChol: Validation, Formal Analysis, Writing - Review & Editing; Ri GiSong: Conceptualization, Methodology, Supervision, Project Administration.. All authors have read and agreed to the published version of the manuscript.

References

[1] Luo, J., Çıtmacı, B., Jang, J.B., Abdullah, F., Morales-Guio, C.G., Christofides, P.D. (2023). Machine learning-based predictive control using on-line model linearization: Application to an experimental electrochemical reactor. *Chemical Engineering Research and Design*, 197, 721-737. DOI: 10.1016/j.cherd.2023.08.017.

[2] Besra, L., Liu, M. (2007). A review on fundamentals and applications of electrophoretic deposition (EPD). *Progress in Materials Science*, 52(1), 1-61. DOI: 10.1016/j.pmatsci.2006.07.001.

[3] Wang, Y., Ahmadkhaniha, D., Sieber, N., Zanella, C. (2024). Controlling coating thickness distribution for a complex geometry using pulse reverse current: A simulation study. *The International Journal of Advanced Manufacturing Technology*, 128, 2409-2423. DOI: 10.1007/s00170-024-12635-4.

[4] Li, M., Shi, D., Christofides, P.D. (2004). Diamond Jet Hybrid HVOF thermal spray: gas-phase and particle behavior modeling and feedback control design. *Industrial & Engineering Chemistry Research*, 43(14), 3632-3652. DOI: 10.1021/ie030559i.

[5] Çıtmacı, B., Luo, J., Jang, J.B. (2022). Machine learning-based ethylene concentration estimation, real-time optimization and feedback control of an experimental electrochemical reactor. *Chemical Engineering Research and Design*, 185, 87-107. DOI: 10.1016/j.cherd.2022.06.044.

[6] Çıtmacı, B., Luo, J., Jang, J.B., Morales-Guio, C.G., Christofides, P.D. (2023). Machine learning-based ethylene and carbon monoxide estimation, real-time optimization, and multivariable feedback control of an experimental electrochemical reactor. *Chemical Engineering Research and Design*, 191, 658-681. DOI: 10.1016/j.cherd.2023.02.003.

[7] Qin, S.J., Badgwell, T.A. (2003). A survey of industrial model predictive control technology. *Control Engineering Practice*, 11(7), 733-764. DOI: 10.1016/S0967-0661(02)00186-7.

[8] Lee, J.H. (2011). Model predictive control: Review of the three decades of development. *International Journal of Control, Automation and Systems*, 9(3), 415-424. DOI: 10.1007/s12555-011-0300-6.

[9] [9]Landau, I.D. (1979). Adaptive Control: The Model Reference Approach. Marcel Dekker. ISBN: 978-0824769468.

[10] Del Rio Chanona, M.E., Wu, Z., Christofides, P.D., Wu, W. (2024). A tutorial review of machine learning-based model predictive control methods. *Reviews in Chemical Engineering*. DOI: 10.1515/revce-2024-0055.

[11] Alhajeri, M.S., Abdullah, F., Wu, Z., Christofides, P.D. (2022). Physics-informed machine learning modeling for predictive control using noisy data. *Chemical Engineering Research and Design*, 186, 34-49. DOI: 10.1016/j.cherd.2022.07.035.

[12] Zou, C., Pramanik, S., Anwar, S. (2020). Electrochemical model based charge optimization for lithium-ion batteries. *IEEE Transactions on Control Systems Technology*, 28(3), 1029-1042. DOI: 10.1109/TCST.2019.2923704.

[13] Abdullah, F., Wu, Z., Christofides, P.D. (2021). Sparse-identification-based model predictive control of nonlinear two-time-scale processes. *Computers & Chemical Engineering*, 153, 107411. DOI: 10.1016/j.compchemeng.2021.107411.

[14] Guduri, B., Batra, R.C. (2022). Adaptive Control of the Atmospheric Plasma Spray Process for Functionally Graded Thermal Barrier Coatings. *Advances in Materials Science and Engineering*, 2022, Article ID 5432541. DOI: 10.1155/2022/5432541.

[15] Guduri, B., Batra, R.C. (2022). Robust model reference adaptive controller for atmospheric plasma spray process. *SN Applied Sciences*, 4, 128. DOI: 10.1007/s42452-022-05012-0.

[16] Åström, K.J., Wittenmark, B. (1995). Adaptive Control (2nd ed.). Addison-Wesley. ISBN: 978-0201558668.

[17] Ioannou, P.A., Sun, J. (1996). Robust Adaptive Control. Prentice Hall. ISBN: 978-0134391007.

[18] Alhajeri, M.S., Wu, Z., Christofides, P.D. (2021). Machine-learning-based state estimation and predictive control of nonlinear processes. *Chemical Engineering Research and Design*, 167, 158-179. DOI: 10.1016/j.cherd.2021.01.009.

[19] Abdullah, F., Christofides, P.D. (2023). Data-based modeling and control of nonlinear process systems using sparse identification: An overview. *Computers & Chemical Engineering*, 174, 108247. DOI: 10.1016/j.compchemeng.2023.108247.

[20] Chen, S., Wu, Z., Christofides, P.D. (2020). Decentralized machine-learning-based predictive control of nonlinear processes. *Chemical Engineering Research and Design*, 160, 80-93. DOI: 10.1016/j.cherd.2020.09.014.

[21] Marusak, P.M. (2020). Numerically Efficient Fuzzy MPC Algorithm with Advanced Generation of Prediction---*Application to a Chemical Reactor*. *Algorithms*, 13(6), 143. DOI: 10.3390/a13060143.

[22] Hong, S., ?ıtmacı, B., Cui, X., Abdullah, F. (2024). Model predictive control of an electrically-heated steam methane reformer. *Digital Chemical Engineering*, 9, 100120. DOI: 10.1016/j.dche.2024.100120.

[23] Dubljevic, S., Christofides, P.D. (2006). Predictive control of parabolic PDEs with boundary control actuation. *Chemical Engineering Science*, 61(18), 6239-6247. DOI: 10.1016/j.ces.2006.05.041.

[24] Li, M., Christofides, P.D. (2004). Feedback control of HVOF thermal spray process accounting for powder size distribution. *Journal of Thermal Spray Technology*, 13(1), 108-120. DOI: 10.1361/10599630418086.

[25] Li, M., Christofides, P.D. (2005). Multi-scale modeling and analysis of an industrial HVOF thermal spray process. *Chemical Engineering Science*, 60(12), 3649-3669. DOI: 10.1016/j.ces.2005.02.043.